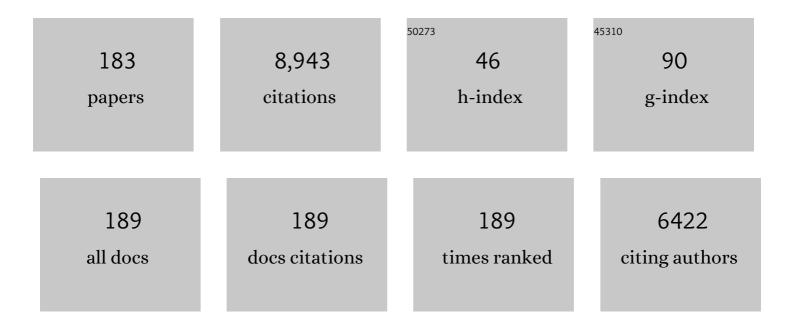
List of Publications by Year in descending order

Source: https://exaly.com/author-pdf/490903/publications.pdf Version: 2024-02-01



PALL ASIMOW

#	Article	IF	CITATIONS
1	Algorithmic modifications extending MELTS to calculate subsolidus phase relations. American Mineralogist, 1998, 83, 1127-1132.	1.9	618
2	Temperatures in ambient mantle and plumes: Constraints from basalts, picrites, and komatiites. Geochemistry, Geophysics, Geosystems, 2007, 8, n/a-n/a.	2.5	571
3	Adiabat_1ph: A new public front-end to the MELTS, pMELTS, and pHMELTS models. Geochemistry, Geophysics, Geosystems, 2005, 6, .	2.5	405
4	Petrology of some oceanic island basalts: PRIMELT2.XLS software for primary magma calculation. Geochemistry, Geophysics, Geosystems, 2008, 9, .	2.5	398
5	The importance of water to oceanic mantle melting regimes. Nature, 2003, 421, 815-820.	27.8	333
6	Emergence of a low-viscosity channel in subduction zones through the coupling of mantle flow and thermodynamics. Earth and Planetary Science Letters, 2009, 278, 243-256.	4.4	327
7	A hydrous melting and fractionation model for mid-ocean ridge basalts: Application to the Mid-Atlantic Ridge near the Azores. Geochemistry, Geophysics, Geosystems, 2004, 5, n/a-n/a.	2.5	281
8	<scp>PRIMELT</scp> 3 <scp>MEGA.XLSM</scp> software for primary magma calculation: Peridotite primary magma MgO contents from the liquidus to the solidus. Geochemistry, Geophysics, Geosystems, 2015, 16, 563-578.	2.5	279
9	Iron isotopes may reveal the redox conditions of mantle melting from Archean to Present. Earth and Planetary Science Letters, 2009, 288, 255-267.	4.4	260
10	Hydrogen incorporation in olivine from 2-12 GPa. American Mineralogist, 2006, 91, 285-294.	1.9	194
11	Contrasting geochemical signatures of fluid-absent versus fluid-fluxed melting of muscovite in metasedimentary sources: The Himalayan leucogranites. Geology, 2017, 45, 39-42.	4.4	184
12	Calculation of Peridotite Partial Melting from Thermodynamic Models of Minerals and Melts. III. Controls on Isobaric Melt Production and the Effect of Water on Melt Production. Journal of Petrology, 1999, 40, 831-851.	2.8	169
13	Calculation of Peridotite Partial Melting from Thermodynamic Models of Minerals and Melts, IV. Adiabatic Decompression and the Composition and Mean Properties of Mid-ocean Ridge Basalts. Journal of Petrology, 2001, 42, 963-998.	2.8	159
14	Calculation of Peridotite Partial Melting from Thermodynamic Models of Minerals and Melts. I. Review of Methods and Comparison with Experiments. Journal of Petrology, 1998, 39, 1091-1115.	2.8	156
15	Coupling of anatectic reactions and dissolution of accessory phases and the Sr and Nd isotope systematics of anatectic melts from a metasedimentary source. Geochimica Et Cosmochimica Acta, 2005, 69, 3671-3682.	3.9	143
16	Toward an international practical pressure scale: A proposal for an IPPS ruby gauge (IPPS-Ruby2020). High Pressure Research, 2020, 40, 299-314.	1.2	143
17	An analysis of variations in isentropic melt productivity. Philosophical Transactions Series A, Mathematical, Physical, and Engineering Sciences, 1997, 355, 255-281.	3.4	133
18	The MgSiO ₃ system at high pressure: Thermodynamic properties of perovskite, postperovskite, and melt from global inversion of shock and static compression data. Journal of Geophysical Research, 2009, 114, .	3.3	120

#	Article	IF	CITATIONS
19	Shock synthesis of quasicrystals with implications for their origin in asteroid collisions. Proceedings of the National Academy of Sciences of the United States of America, 2016, 113, 7077-7081.	7.1	112
20	Nd isotope disequilibrium during crustal anatexis: A record from the Goat Ranch migmatite complex, southern Sierra Nevada batholith, California. Geology, 2005, 33, 53.	4.4	99
21	Analysis of hydrogen in olivine by SIMS: Evaluation of standards and protocol. American Mineralogist, 2011, 96, 1725-1741.	1.9	98
22	The effect of pressure-induced solid-solid phase transitions on decompression melting of the mantle. Geochimica Et Cosmochimica Acta, 1995, 59, 4489-4506.	3.9	95
23	Shock-induced melting of MgSiO3perovskite and implications for melts in Earth's lowermost mantle. Geophysical Research Letters, 2004, 31, .	4.0	93
24	Thermodynamic properties of Mg2SiO4liquid at ultra-high pressures from shock measurements to 200 GPa on forsterite and wadsleyite. Journal of Geophysical Research, 2007, 112, .	3.3	92
25	Cation field strength effects on high pressure aluminosilicate glass structure: Multinuclear NMR and La XAFS results. Geochimica Et Cosmochimica Acta, 2009, 73, 3914-3933.	3.9	88
26	Steady-state Mantle-Melt Interactions in One Dimension: I. Equilibrium Transport and Melt Focusing. Journal of Petrology, 1999, 40, 475-494.	2.8	86
27	A model that reconciles major- and trace-element data from abyssal peridotites. Earth and Planetary Science Letters, 1999, 169, 303-319.	4.4	83
28	Room-Temperature Pressure Synthesis of Layered Black Phosphorus–Graphene Composite for Sodium-Ion Battery Anodes. ACS Nano, 2018, 12, 8323-8329.	14.6	83
29	Identifying high potential zones of gold mineralization in a sub-tropical region using Landsat-8 and ASTER remote sensing data: A case study of the Ngoura-Colomines goldfield, eastern Cameroon. Ore Geology Reviews, 2020, 122, 103530.	2.7	83
30	Nickel and helium evidence for melt above the core–mantle boundary. Nature, 2013, 493, 393-397.	27.8	77
31	Origins of chemical diversity of backâ€arc basin basalts: A segmentâ€scale study of the Eastern Lau Spreading Center. Journal of Geophysical Research, 2009, 114, .	3.3	76
32	Multiâ€ŧechnique equation of state for Fe ₂ SiO ₄ melt and the density of Feâ€bearing silicate melts from 0 to 161 GPa. Journal of Geophysical Research, 2012, 117, .	3.3	76
33	Quantitative polarized infrared analysis of trace OH in populations of randomly oriented mineral grains. American Mineralogist, 2006, 91, 278-284.	1.9	74
34	Effect of Al on the sharpness of the MgSiO3perovskite to post-perovskite phase transition. Geophysical Research Letters, 2005, 32, n/a-n/a.	4.0	71
35	Simultaneous aluminum, silicon, and sodium coordination changes in 6 GPa sodium aluminosilicate glasses. American Mineralogist, 2009, 94, 1205-1215.	1.9	70
36	Shock-compressed MgSiO3glass, enstatite, olivine, and quartz: Optical emission, temperatures, and melting. Journal of Geophysical Research, 2004, 109, .	3.3	69

#	Article	IF	CITATIONS
37	A model for rutile saturation in silicate melts with applications to eclogite partial melting in subduction zones and mantle plumes. Earth and Planetary Science Letters, 2008, 272, 720-729.	4.4	68
38	Zonation of H2O and F Concentrations around Melt Inclusions in Olivines. Journal of Petrology, 2014, 55, 685-707.	2.8	68
39	Neoproterozoic boninite-series rocks in South China: A depleted mantle source modified by sediment-derived melt. Chemical Geology, 2014, 388, 98-111.	3.3	67
40	The Significance of Multiple Saturation Points in the Context of Polybaric Near-fractional Melting. Journal of Petrology, 2004, 45, 2349-2367.	2.8	66
41	Enhanced East Pacific Rise hydrothermal activity during the last two glacial terminations. Science, 2016, 351, 478-482.	12.6	64
42	Oxygen isotope evidence for the origin of enriched mantle beneath the mid-Atlantic ridge. Earth and Planetary Science Letters, 2004, 220, 297-316.	4.4	63
43	An Andean-type arc system in Rodinia constrained by the Neoproterozoic Shimian ophiolite in South China. Precambrian Research, 2017, 296, 93-111.	2.7	63
44	Partial melting of deeply subducted continental crust and the formation of quartzofeldspathic polyphase inclusions in the Sulu UHP eclogites. Science Bulletin, 2009, 54, 2580-2594.	9.0	62
45	Does sea level influence mid-ocean ridge magmatism on Milankovitch timescales?. Geochemistry, Geophysics, Geosystems, 2011, 12, n/a-n/a.	2.5	51
46	Formation and Evolution of a Magmatic System in a Rifting Continental Margin: Neoproterozoic Arc- and MORB-like Dike Swarms in South China. Journal of Petrology, 2018, 59, 1811-1844.	2.8	50
47	Direct shock wave loading of Stishovite to 235 GPa: Implications for perovskite stability relative to an oxide assemblage at lower mantle conditions. Geophysical Research Letters, 2002, 29, 36-1-36-4.	4.0	46
48	Generation of talc in the mantle wedge and its role in subduction dynamics in central Mexico. Earth and Planetary Science Letters, 2013, 384, 81-87.	4.4	46
49	Laser-induced shock waves in condensed matter: some techniques and applications. High Pressure Research, 2004, 24, 409-422.	1.2	44
50	Shock compression of liquid silicates to 125 GPa: The anorthiteâ€diopside join. Journal of Geophysical Research, 2010, 115, .	3.3	44
51	Polymorphism, superheating, and amorphization of silica upon shock wave loading and release. Journal of Geophysical Research, 2003, 108, .	3.3	42
52	Direct shock compression experiments on premolten forsterite and progress toward a consistent highâ€pressure equation of state for CaOâ€MgOâ€Al ₂ O ₃ â€SiO ₂ â€FeO liquids. Journal of Geophysical Research: Solid Earth, 2013, 118, 5738-5752.	3.4	42
53	Hydrous, Low-carbon Melting of Garnet Peridotite. Journal of Petrology, 2011, 52, 2079-2105.	2.8	40
54	High pressure minerals in the Château-Renard (L6) ordinary chondrite: implications for collisions on its parent body. Scientific Reports, 2018, 8, 9851.	3.3	39

#	Article	IF	CITATIONS
55	Water-in-olivine magma ascent chronometry: Every crystal is a clock. Journal of Volcanology and Geothermal Research, 2020, 398, 106872.	2.1	39
56	Insights into mantle melting from graphical analysis of one-component systems. Numerische Mathematik, 2007, 307, 1051-1139.	1.4	38
57	Molybdenum sound velocity and shear modulus softening under shock compression. Physical Review B, 2014, 89, .	3.2	37
58	Ultrafast growth of wadsleyite in shock-produced melts and its implications for early solar system impact processes. Proceedings of the National Academy of Sciences of the United States of America, 2009, 106, 13691-13695.	7.1	36
59	A double-spike method for K–Ar measurement: A technique for high precision in situ dating on Mars and other planetary surfaces. Geochimica Et Cosmochimica Acta, 2013, 110, 1-12.	3.9	30
60	The late Neoproterozoic Dahanib mafic-ultramafic intrusion, South eastern Desert, Egypt: Is it an Alaskan-type or a layered intrusion?. Numerische Mathematik, 2017, 317, 901-940.	1.4	30
61	Manganese partitioning during hydrous melting of peridotite. Geochimica Et Cosmochimica Acta, 2011, 75, 5819-5833.	3.9	29
62	Calculation of Peridotite Partial Melting from Thermodynamic Models of Minerals and Melts. III. Controls on Isobaric Melt Production and the Effect of Water on Melt Production. Journal of Petrology, 1999, 40, 831-851.	2.8	29
63	Determination of the partial molar volume of SiO2 in silicate liquids at elevated pressures and temperatures: a new experimental approach. Geochimica Et Cosmochimica Acta, 1998, 62, 2499-2508.	3.9	27
64	On the relative timing of listwaenite formation and chromian spinel equilibration in serpentinites. American Mineralogist, 2018, 103, 1087-1102.	1.9	27
65	Multiple Stages of Carbonation and Element Redistribution during Formation of Ultramafic-Hosted Magnesite in Neoproterozoic Ophiolites of the Arabian-Nubian Shield, Egypt. Journal of Geology, 2019, 127, 81-107.	1.4	27
66	Tracking the transition from subductionâ€related to postâ€collisional magmatism in the north Arabian–Nubian Shield: A case study from the Homrit Waggat area of the Eastern Desert of Egypt. Geological Journal, 2020, 55, 4426-4452.	1.3	27
67	Steady-state Mantle-Melt Interactions in One Dimension: II. Thermal Interactions and Irreversible Terms. Journal of Petrology, 2002, 43, 1707-1724.	2.8	26
68	Grain boundary partitioning of Ar and He. Geochimica Et Cosmochimica Acta, 2007, 71, 434-451.	3.9	26
69	Highly CO2-supersaturated melts in the Pannonian lithospheric mantle – A transient carbon reservoir?. Lithos, 2017, 286-287, 519-533.	1.4	26
70	Geochemistry and petrogenesis of post-collisional alkaline and peralkaline granites of the Arabian-Nubian Shield: a case study from the southern tip of Sinai Peninsula, Egypt. International Geology Review, 2018, 60, 998-1018.	2.1	26
71	A new dense silica polymorph: A possible link between tetrahedrally and octahedrally coordinated silica. American Mineralogist, 2004, 89, 455-461.	1.9	25
72	Recovery of stishovite-structure at ambient conditions out of shock-generated amorphous silica. American Mineralogist, 2006, 91, 1857-1862.	1.9	25

#	Article	IF	CITATIONS
73	Secondary fluorescence effects in microbeam analysis and their impacts on geospeedometry and geothermometry. Chemical Geology, 2018, 490, 22-29.	3.3	25
74	Fluid outflows from Venus impact craters: Analysis from Magellan data. Journal of Geophysical Research, 1992, 97, 13643-13665.	3.3	24
75	Experimental study of radium partitioning between anorthite and melt at 1 atm. American Mineralogist, 2007, 92, 1535-1538.	1.9	23
76	High frequency seismic waves and slab structures beneath Italy. Earth and Planetary Science Letters, 2014, 391, 212-223.	4.4	23
77	Determination of melt influence on divalent element partitioning between anorthite and CMAS melts. Geochimica Et Cosmochimica Acta, 2006, 70, 4258-4274.	3.9	22
78	Cation order/disorder behavior and crystal chemistry of pyrope-grossular garnets: An 17O 3QMAS and 27Al MAS NMR spectroscopic study. American Mineralogist, 2008, 93, 134-143.	1.9	22
79	Shock compression of preheated molybdenum to 300GPa. Physics of the Earth and Planetary Interiors, 2009, 174, 302-308.	1.9	22
80	Shock Synthesis of Five-component Icosahedral Quasicrystals. Scientific Reports, 2017, 7, 15629.	3.3	22
81	Shock Synthesis of Decagonal Quasicrystals. Scientific Reports, 2017, 7, 15628.	3.3	21
82	Early Cretaceous high-Ti and low-Ti mafic magmatism in Southeastern Tibet: Insights into magmatic evolution of the Comei Large Igneous Province. Lithos, 2018, 296-299, 396-411.	1.4	21
83	Geochemistry of middle-late Mesozoic mafic intrusions in the eastern North China Craton: New insights on lithospheric thinning and decratonization. Gondwana Research, 2019, 73, 153-174.	6.0	21
84	High-pressure melt curve of shock-compressed tin measured using pyrometry and reflectance techniques. Journal of Applied Physics, 2019, 126, .	2.5	21
85	Configurational entropy of basaltic melts in Earth's mantle. Proceedings of the National Academy of Sciences of the United States of America, 2020, 117, 21938-21944.	7.1	21
86	Thermodynamic properties of alloys of gold-74/palladium-26 with variable amounts of iron and the use of Au-Pd-Fe alloys as containers for experimental petrology. American Mineralogist, 2011, 96, 1467-1474.	1.9	20
87	Hydrogen Incorporation in Natural Mantle Olivines. Geophysical Monograph Series, 0, , 45-56.	0.1	20
88	Seconds after impact: Insights into the thermal history of impact ejecta from diffusion between lechatelierite and host glass in tektites and experiments. Geochimica Et Cosmochimica Acta, 2018, 241, 69-94.	3.9	20
89	The last subduction-related volcanism in the northern tip of the Arabian-Nubian Shield: A Neoproterozoic arc preceding the terminal collision of East and West Gondwana. Precambrian Research, 2018, 310, 256-277.	2.7	18
90	Late Neoproterozoic adakitic lavas in the Arabian-Nubian shield, Sinai Peninsula, Egypt. Journal of Asian Earth Sciences, 2018, 158, 301-323.	2.3	17

#	Article	IF	CITATIONS
91	PetroPlot: A plotting and data management tool set for Microsoft Excel. Geochemistry, Geophysics, Geosystems, 2003, 4, .	2.5	16
92	Mineral chemistry of the Tissint meteorite: Indications of twoâ€stage crystallization in a closed system. Meteoritics and Planetary Science, 2016, 51, 2293-2315.	1.6	16
93	Tantalum sound velocity under shock compression. Journal of Applied Physics, 2019, 125, .	2.5	16
94	The effects of solid-solid phase equilibria on the oxygen fugacity of the upper mantle. American Mineralogist, 2020, 105, 1445-1471.	1.9	16
95	Accidental synthesis of a previously unknown quasicrystal in the first atomic bomb test. Proceedings of the National Academy of Sciences of the United States of America, 2021, 118, .	7.1	16
96	Late Ediacaran post-collisional A-type syenites with shoshonitic affinities, northern Arabian-Nubian Shield: a possible mantle-derived A-type magma. Arabian Journal of Geosciences, 2016, 9, 1.	1.3	15
97	Stishovite and its implications in geophysics: new results from shock-wave experiments and theoretical modeling. Physics-Uspekhi, 2002, 45, 435-439.	2.2	14
98	Fluid source-based modeling of melt initiation within the subduction zone mantle wedge: Implications for geochemical trends in arc lavas. Chemical Geology, 2009, 266, 297-310.	3.3	14
99	Current limitations of molecular dynamic simulations as probes of thermo-physical behavior of silicate melts. American Mineralogist, 2015, 100, 1866-1882.	1.9	14
100	Thermodynamically complete equation of state of MgO from true radiative shock temperature measurements on samples preheated to 1850 K. Physical Review B, 2018, 97, .	3.2	14
101	The Atud gabbro–diorite complex: glimpse of the Cryogenian mixing, assimilation, storage and homogenization zone beneath the Eastern Desert of Egypt. Journal of the Geological Society, 2020, 177, 965-980.	2.1	14
102	Genesis and geodynamic evolution of serpentinized ultramafics and associated magnesite deposits in the Al-Wask ophiolite, Arabian Shield, Saudi Arabia. Numerische Mathematik, 2020, 320, 236-279.	1.4	14
103	Magmatic and post-magmatic evolution of post-collisional rare-metal bearing granite: The Neoproterozoic Homrit Akarem Granitic Intrusion, south Eastern Desert of Egypt, Arabian-Nubian Shield. Chemie Der Erde, 2022, 82, 125840.	2.0	14
104	Ab initio study of the structure and stability of CaMg(CO ₃) ₂ at high pressure. American Mineralogist, 2017, 102, 210-215.	1.9	13
105	An example of post-collisional appinitic magmatism with an arc-like signature: the Wadi Nasb mafic intrusion, north Arabian–Nubian Shield, south Sinai, Egypt. International Geology Review, 2018, 60, 865-888.	2.1	13
106	Hydrothermal scavenging of 230Th on the Southern East Pacific Rise during the last deglaciation. Earth and Planetary Science Letters, 2019, 510, 64-72.	4.4	13
107	Petrological characteristics of the Neoproterozoic Ess ophiolite mantle section, Arabian Shield, Saudi Arabia: a mineral chemistry perspective. International Journal of Earth Sciences, 2020, 109, 239-251.	1.8	13
108	First synthesis of a unique icosahedral phase from the Khatyrka meteorite by shock-recovery experiment. IUCrJ, 2020, 7, 434-444.	2.2	13

#	Article	IF	CITATIONS
109	Structure of shock compressed model basaltic glass: Insights from O Kâ€edge Xâ€ray Raman scattering and highâ€resolution ²⁷ Al NMR spectroscopy. Geophysical Research Letters, 2012, 39, .	4.0	12
110	Mid-Neoproterozoic mafic rocks in the western Jiangnan orogen, South China: Intracontinental rifting or subduction?. Journal of Asian Earth Sciences, 2019, 185, 104039.	2.3	12
111	Novel crystalline carbon-cage structure synthesized from laser-driven shock wave loading of graphite. Journal of Chemical Physics, 2005, 123, 024703.	3.0	11
112	Equation of state of liquid bismuth and its melting curve from ultrasonic investigation at high pressure. Physica B: Condensed Matter, 2017, 524, 154-162.	2.7	11
113	First-principles calculations of high-pressure iron-bearing monoclinic dolomite and single-cation carbonates with internally consistent Hubbard U. Physics and Chemistry of Minerals, 2018, 45, 293-302.	0.8	11
114	The potential of phosphorus in clinopyroxene as a geospeedometer: Examples from mantle xenoliths. Geochimica Et Cosmochimica Acta, 2019, 266, 307-331.	3.9	11
115	Application of Al-Cu-W-Ta graded density impactors in dynamic ramp compression experiments. Journal of Applied Physics, 2019, 125, .	2.5	11
116	Suprasubduction-zone origin of the podiform chromitites of the Bir Tuluhah ophiolite, Saudi Arabia, during Neoproterozoic assembly of the Arabian Shield. Lithos, 2020, 360-361, 105439.	1.4	11
117	Late Cretaceous adakitic and A-type granitoids in Chanang, southern Tibet: Implications for Neo-Tethyan slab rollback. Gondwana Research, 2021, 96, 89-104.	6.0	11
118	Tests of random density models of terrestrial planets. Geophysical Research Letters, 1991, 18, 909-912.	4.0	10
119	Preheated shock experiments in the molten CaAl ₂ Si ₂ O ₈ â€CaFeSi ₂ O ₆ â€CaMgSi _{2ternary: A test for linear mixing of liquid volumes at high pressure and temperature. Journal of Geophysical Research: Solid Earth, 2013, 118, 3354-3365.}	sub _{3.} 9 <sut< td=""><td>o>6{/sub></td></sut<>	o>6{/sub>
120	Coordinated Hard Sphere Mixture (CHaSM): A simplified model for oxide and silicate melts at mantle pressures and temperatures. Geochimica Et Cosmochimica Acta, 2015, 163, 40-58.	3.9	10
121	Geochemistry of the Serifos calc-alkaline granodiorite pluton, Greece: constraining the crust and mantle contributions to I-type granitoids. International Journal of Earth Sciences, 2018, 107, 1657-1688.	1.8	10
122	Geochemistry and Petrogenesis of Late Ediacaran Rareâ€metal Albite Granites of the Arabianâ€Nubian Shield. Acta Geologica Sinica, 2021, 95, 459-480.	1.4	10
123	Petrogenesis of Ultramafic Rocks from the Ultrahigh-pressure Metamorphic Kimi Complex in Eastern Rhodope (NE Greece). Journal of Petrology, 2008, 49, 885-909.	2.8	9
124	Contributed Review: Absolute spectral radiance calibration of fiber-optic shock-temperature pyrometers using a coiled-coil irradiance standard lamp. Review of Scientific Instruments, 2015, 86, 101502.	1.3	9
125	Phosphorus zoning as a recorder of crystal growth kinetics: application to second-generation olivine in mantle xenoliths from the Cima Volcanic Field. Contributions To Mineralogy and Petrology, 2017, 172, 1.	3.1	9
126	Petrogenesis of gold-bearing listvenites from the carbonatized mantle section of the Neoproterozoic Ess ophiolite, Western Arabian Shield, Saudi Arabia. Lithos, 2020, 372-373, 105679.	1.4	9

#	Article	IF	CITATIONS
127	Oxygen isotope constraints on the structure and evolution of the Hawaiian Plume. Numerische Mathematik, 2010, 310, 683-720.	1.4	8
128	MgO melting curve constraints from shock temperature and rarefaction overtake measurements in samples preheated to 2300 K. Journal of Physics: Conference Series, 2014, 500, 062003.	0.4	8
129	Ultramafic lavas and high-Mg basaltic dykes from the Othris ophiolite complex, Greece. Lithos, 2017, 288-289, 231-247.	1.4	8
130	In Situ Observations of Phase Changes in Shock Compressed Forsterite. Geophysical Research Letters, 2018, 45, 8129-8135.	4.0	8
131	Crystal size distribution of amphibole grown from hydrous basaltic melt at 0.6–2.6 GPa and 860–970 °C. American Mineralogist, 2019, 104, 525-535.	1.9	8
132	The common origin and alteration history of the hypabyssal and volcanic phases of the Wadi Tarr albitite complex, southern Sinai, Egypt. Lithos, 2019, 324-325, 821-841.	1.4	8
133	Post-collisional volcanism with adakitic signatures in the Arabian-Nubian Shield: A case study of calc-alkaline Dokhan volcanics in the Eastern Desert of Egypt. Lithos, 2021, 388-389, 106051.	1.4	8
134	Experimental constraints on truly conjugate alkaline silicate – carbonatite melt pairs. Earth and Planetary Science Letters, 2022, 584, 117500.	4.4	8
135	Anomalous Pacificâ€Antarctic Ridge Volcanism Precedes Glacial Termination 2. Geochemistry, Geophysics, Geosystems, 2018, 19, 2478-2491.	2.5	7
136	Mineralogical and geochemical study of rodingites and associated serpentinized peridotite, Eastern Desert of Egypt, Arabian-Nubian Shield. Lithos, 2020, 374-375, 105720.	1.4	7
137	Femtosecond Xâ€Ray Diffraction of Laserâ€5hocked Forsterite (Mg ₂ SiO ₄) to 122ÂGPa. Journal of Geophysical Research: Solid Earth, 2021, 126, .	3.4	7
138	Petrogenetic Evolution of the Neoproterozoic Igneous Rocks of Egypt. Regional Geology Reviews, 2021, , 343-382.	1.2	7
139	Formation of gold-bearing listvenite in the mantle section of the Neoproterozoic Bir Umq ophiolite, Western Arabian Shield, Saudi Arabia. Journal of African Earth Sciences, 2022, 190, 104517.	2.0	7
140	Shock compression of preheated silicate liquids: Apparent universality of increasing GruÌ^neisen parameter upon compression. , 2012, , .		6
141	The molar volume of FeO–MgO–Fe2O3–Cr2O3–Al2O3–TiO2 spinels. Contributions To Mineralogy and Petrology, 2013, 165, 25.	3.1	6
142	Continental rift and oceanic protoliths of mafic–ultramafic rocks from the Kechros Complex, NE Rhodope (Greece): implications from petrography, major and trace-element systematics, and MELTS modeling. International Journal of Earth Sciences, 2014, 103, 981-1003.	1.8	6
143	Reply to "Comment on â€~Molybdenum sound velocity and shear modulus softening under shock compression' ― Physical Review B, 2015, 92, .	3.2	6
144	A self-consistent optimization of multicomponent solution properties: Ab initio molecular dynamic simulations and the MgO–SiO2 miscibility gap under pressure. Geochimica Et Cosmochimica Acta, 2015, 161, 146-165.	3.9	6

#	Article	IF	CITATIONS
145	Geophysical source conditions for basaltic lava from Santorini volcano based on geochemical modeling. Lithos, 2018, 316-317, 295-303.	1.4	6
146	Trace Element Conundrum of Natural Quasicrystals. ACS Earth and Space Chemistry, 2021, 5, 676-689.	2.7	6
147	Shock-synthesized glassy and solid silica: intermediates between four- and six-fold coordination. High Pressure Research, 2004, 24, 471-479.	1.2	5
148	Equation of state of Mo from shock compression experiments on preheated samples. Journal of Applied Physics, 2017, 121, .	2.5	5
149	Melts Under Extreme Conditions From Shock Experiments. , 2018, , 387-418.		5
150	Microtextures in the Chelyabinsk impact breccia reveal the history of Phosphorusâ€Olivineâ€Assemblages in chondrites. Meteoritics and Planetary Science, 2021, 56, 742-766.	1.6	5
151	SHOCK TEMPERATURES OF PREHEATED MgO. , 2009, , .		4
152	A measure of mantle melting. Science, 2017, 355, 908-909.	12.6	4
153	Petrogenesis of the post-collisional rare-metal-bearing Ad-Dayheen granite intrusion, Central Arabian Shield. Lithos, 2021, 384-385, 105956.	1.4	4
154	Evolution of a Neoproterozoic island arc in the northern Arabian-Nubian Shield: Volcanic rocks and their plutonic equivalents in the Hamash area, south Eastern Desert, Egypt. Precambrian Research, 2021, 358, 106145.	2.7	4
155	Two episodes of Eocene mafic magmatism in the southern Lhasa terrane imply an eastward propagation of slab breakoff. Gondwana Research, 2022, 110, 31-43.	6.0	4
156	Time-Resolved X-Ray Diffraction Investigation of Superheating-Melting of Crystals under Ultrafast Heating. AIP Conference Proceedings, 2004, , .	0.4	3
157	Advances in high-pressure mineral physics: From the deep mantle to the core. Physics of the Earth and Planetary Interiors, 2009, 174, 1-2.	1.9	3
158	Prehnite as an indicator mineral in the Wadi Nasb uralitized gabbro, South Sinai, Egypt. Journal of Asian Earth Sciences, 2018, 160, 107-117.	2.3	3
159	Late Cretaceous Construction of the Mantle Lithosphere Beneath the Central California Coast Revealed by Crystal Knob Xenoliths. Geochemistry, Geophysics, Geosystems, 2018, 19, 3302-3346.	2.5	3
160	Santorini volcano as a potential Martian analogue: The Balos Cove Basalts. Icarus, 2019, 325, 128-140.	2.5	3
161	A slice of history. Nature, 2003, 423, 491-492.	27.8	2
162	Volcanism During the Post-accretionary Stage of the Arabian–Nubian Shield. Regional Geology Reviews, 2021, , 485-533.	1.2	2

PAUL ASIMOW

#	Article	IF	CITATIONS
163	Neoproterozoic Ophiolites of the Arabian-Nubian Shield. Regional Geology Reviews, 2021, , 297-330.	1.2	2
164	Geochemistry and mineralogy of the Jebel Aja Igneous Intrusion and the associated exotic pegmatites, Arabian Shield, Saudi Arabia. Lithos, 2021, 400-401, 106395.	1.4	2
165	Partial Melting. Encyclopedia of Earth Sciences Series, 2016, , 1-6.	0.1	2
166	The Mantle Section of Neoproterozoic Ophiolites from the Pan-African Belt, Eastern Desert, Egypt: Tectonomagmatic Evolution, Metamorphism, and Mineralization. Regional Geology Reviews, 2021, , 309-341.	1.2	2
167	Multistage petrogenetic evolution of Neoproterozoic serpentinized ultramafic rocks and podiform chromitites at Hagar Dungash, Eastern Desert of Egypt. Precambrian Research, 2022, 369, 106507.	2.7	2
168	A multi-phase field model for mesoscopic interface dynamics with large bulk driving forces. Computational Materials Science, 2022, 212, 111570.	3.0	2
169	Synthesis and thermoelectric properties of Ce(Ru0.67Rh0.33)4Sb12 Materials Research Society Symposia Proceedings, 2003, 793, 176.	0.1	1
170	ADVANCES IN SHOCK COMPRESSION OF MANTLE MINERALS AND IMPLICATIONS. , 2009, , .		1
171	An internal energy-dependent model for the Grüneisen parameter of silicate liquids. Geochimica Et Cosmochimica Acta, 2022, 316, 59-68.	3.9	1
172	Tectonochemistry of the Brooks Range Ophiolite, Alaska. Lithosphere, 2020, 2020, .	1.4	1
173	The kabr El-Bonaya peridotites, Southeastern Sinai, Egypt: petrology, geochemistry, and metamorphism of Neoproterozoic arc ultramafic cumulates. Numerische Mathematik, 2021, 321, 1445-1496.	1.4	1
174	Shock experiments on basalt—Ferric sulfate mixes and their possible relevance to the sulfide bleb clusters in large impact melts in shergottites. Meteoritics and Planetary Science, 2021, 56, 2250-2264.	1.6	1
175	Unique evidence of fluid alteration in the Kakowa (L6) ordinary chondrite. Scientific Reports, 2022, 12, 5520.	3.3	1
176	Acceptance of the 2003 F. W. Clarke Award. Geochimica Et Cosmochimica Acta, 2004, 68, 1965-1966.	3.9	0
177	Asimow, Jahren, and Randerson receive 2005 James B. Macelwane Medal. Eos, 2006, 87, 40.	0.1	0
178	(Invited) Novel Applications of Knudsen Effusion Mass Spectrometry. ECS Transactions, 2013, 58, 3-12.	0.5	0
179	A lesson in defining "extinct― Physics Today, 2014, 67, 8-8.	0.3	0
180	Thermodynamic Modeling of Silicate Systems. , 2021, , 44-51.		0

11

#	Article	IF	CITATIONS
181	Partial Melting. Encyclopedia of Earth Sciences Series, 2018, , 1180-1185.	0.1	Ο
182	Shock synthesis of Al-Fe-Cr-Cu-Ni icosahedral quasicrystal. AIP Conference Proceedings, 2020, , .	0.4	0
183	Thank You to Our 2021 Reviewers. Geochemistry, Geophysics, Geosystems, 2022, 23, .	2.5	0